Geophysical Research Letters

RESEARCH LETTER
10.1029/2024GL114187

Key Points:

- Initial scientific work to present temporal and spatial gravity wave (GW) variations at ~87 km observed by the NASA AWE mission
- Reduced GW activity following the 2024 Sudden Stratospheric Warmings was observed by AWE
- The decline in GW activity was most likely caused by wind filtering and wave saturation

Correspondence to:
J. Zhang,
jiarong.zhang@usu.edu

Citation:
Zhang, J., Zhao, Y., Pautet, P.-D., Scherliess, L., Taylor, M. J., & Liu, H. (2025). Gravity wave activity during the 2024 sudden stratospheric warmings observed by atmospheric waves experiment (AWE). *Geophysical Research Letters*, *52*, e2024GL114187. https://doi.org/10.1029/2024GL114187

Received 17 DEC 2024
Accepted 12 MAR 2025

Author Contributions:
Conceptualization: Jiarong Zhang
Formal analysis: Jiarong Zhang
Funding acquisition: Michael J. Taylor
Methodology: Jiarong Zhang, Yucheng Zhao, Pierre-Dominique Pautet, Ludger Scherliess
Software: Pierre-Dominique Pautet
Visualization: Jiarong Zhang
Writing – original draft: Jiarong Zhang
Writing – review & editing: Jiarong Zhang, Yucheng Zhao, Pierre-Dominique Pautet, Ludger Scherliess, Hanli Liu

Gravity Wave Activity During the 2024 Sudden Stratospheric Warmings Observed by Atmospheric Waves Experiment (AWE)

Jiarong Zhang[1], Yucheng Zhao[1], Pierre-Dominique Pautet[1], Ludger Scherliess[1], Michael J. Taylor[1], and Hanli Liu[2]

[1]Department of Physics, Utah State University, Logan, UT, USA, [2]High Altitude Observatory, NSF National Center for Atmospheric Research, Boulder, CO, USA

Abstract The National Aeronautics and Space Administration (NASA) Atmospheric Waves Experiment (AWE) instrument, launched in November 2023, provides direct observation of small-scale (30–300 km) gravity waves (GWs) in the mesosphere on a global scale. This work examined changes in GW activity observed by AWE during two major Sudden Stratospheric Warmings (SSWs) in the 2023 and 2024 winter season. Northern Hemisphere (NH) midlatitude GW activity during these events shared similarities. Variations in mesospheric GW activity showed an evident correlation with the magnitude of zonal wind in the upper stratosphere. NH midlatitude GW activity at ~87 km was reduced following the onset of SSWs, likely caused by wind filtering and wave saturation. The upward propagation of GWs was suppressed when the zonal wind reversed from eastward to westward in the upper stratosphere. In regions where the zonal wind weakened but remained eastward, the weakened GWs could be due to their refraction to shorter vertical wavelengths.

Plain Language Summary Atmospheric gravity waves (GWs) are buoyancy waves with horizontal wavelengths ranging from tens to thousands of kilometers. The National Aeronautics and Space Administration (NASA) Atmospheric Waves Experiment (AWE) mission was launched to the International Space Station (ISS) in November 2023, providing global observations of small-scale (30–300 km) GWs at ~87 km. Two major sudden stratospheric warmings (SSWs) occurred during the winter of 2023 and 2024 after the AWE instrument was launched. SSWs are large-scale meteorological phenomenon in the stratosphere, characterized by rapid increases in temperature over several days. In this study, we found that the changes in GW activity observed by AWE during these two SSWs were similar. The reversal of zonal wind from eastward to westward in the upper stratosphere during the SSWs suppressed the upward propagation of GWs. As a result, NH midlatitude GW activity at ~87 km was reduced. In some regions where zonal wind remained weakly eastward, GWs were also weakened due to their refraction to shorter vertical wavelengths. This is the first study to present temporal and spatial GW variations observed by AWE during the major SSW events of 2024.

1. Introduction

Atmospheric gravity waves (GWs) are generated by various tropospheric sources such as orography, jet stream, and convection (Holton, 1983; Lindzen, 1981). GWs may also be excited by spontaneous adjustment of the strong winter stratospheric jet polar vortex (Sato, 2000; Sato & Yoshiki, 2008). The amplitude of GWs grows exponentially as they propagate to higher altitudes. In the mesosphere and lower thermosphere (MLT), at altitudes of typically 50–130 km, a large fraction of upward-propagating GWs reach a critical level where they break and/or dissipate (Fritts & Alexander, 2003). The deposited momentum and energy drive the summer-to-winter, pole-to-pole mean meridional circulation that gives rise to the thermal structure of the mesosphere (Andrews et al., 1987; Fritts & Alexander, 2003; Kim et al., 2003). Therefore, GWs are recognized as one of the primary components of atmospheric dynamics, particularly for the middle atmosphere.

GW variations have been studied through various observations and numerical simulations. Ground-based measurements include airglow images (Cao & Liu, 2022; Hecht et al., 2023; Taylor et al., 2019), radars (Beldon & Mitchell, 2009, 2010; Dowdy et al., 2007; Hibbins et al., 2007; Mitchell & Beldon, 2009; I. S. Song et al., 2017; B. G. Song et al., 2021; Vincent, 1994; Vincent & Fritts, 1987; Vincent & Reid, 1983), lidars (S. P. Alexander et al., 2011; Beatty et al., 1992; Chanin & Hauchecorne, 1981; T. Li et al., 2010; Wilson et al., 1991; Yamashita et al., 2009; Yuan et al., 2016), and radiosonde (Z. Li et al., 2009; Wang & Geller, 2003; Wang et al., 2005;

Yoshiki & Sato, 2000). However, the ground-based observations provide only limited spatial coverage and for most of them require clear air conditions, which makes it difficult to observe GWs from convective sources (Yue et al., 2013). Spaceborne observations have helped construct global maps of GW activity, such as the Limb Infrared Monitor of the Stratosphere (LIMS) (Fetzer & Gille, 1994), the Cryogenic Infrared Spectrometers and Telescopes for the Atmosphere (CRISTA) (Ern, 2004; Preusse et al., 1999, 2000, 2002), the Microwave Limb Sounder (MLS) on board the Upper Atmosphere Research Satellite (UARS) (McLandress et al., 2000; Wu & Waters, 1996a, 1996b, 1997), Global Positioning System (GPS) radio occultations (De la Torre et al., 2004; Tsuda et al., 2000), the High Resolution Dynamics Limb Sounder (HIRDLS) (M. J. Alexander et al., 2008), and the Sounding of the Atmosphere using Broadband Emission Radiometry (SABER) on the Thermosphere, Ionosphere, Mesosphere Energetics Dynamics (TIMED) satellite (Ern et al., 2011; Preusse et al., 2009; Zhang et al., 2012). These instruments are sensitive to GWs with short vertical wavelengths, whereas their sensitivity to waves with short horizontal wavelengths is limited due to the viewing geometry (Hozumi et al., 2024). In contrast, nadir-viewing instruments have high horizontal resolution to detect GWs with short horizontal wavelengths. Stratospheric GWs on a global scale have been revealed in the Atmospheric Infrared Sounder (AIRS) aboard the Aqua satellite (Ern et al., 2017; Hoffmann et al., 2013, 2016) and the Cloud Imaging and Particle Size (CIPS) instrument on the Aeronomy of Ice in the Mesosphere (AIM) satellite (Harvey et al., 2023; Randall et al., 2017). However, detailed global information about GWs with short horizontal wavelengths in the mesosphere remains limited. The Day/Night Band (DNB) sensor onboard the Suomi National Polar-orbiting Partnership (SNPP) satellite (Azeem et al., 2015) and the Ionosphere, Mesosphere, upper Atmosphere, and Plasmasphere mapping (IMAP)/Visible and near-Infrared Spectral Imager (VISI) (Perwitasari et al., 2015) have revealed numerous concentric GW events in the mesosphere. Recent developments of high-resolution whole atmosphere general circulation models made it possible to resolve a large portion of the GW spectrum and thus enabled the study of GW variation from the Earth surface to the middle or even upper atmosphere (e.g., Becker & Vadas, 2018; Liu et al., 2014; Liu et al., 2024; Siskind et al., 2010; Yamashita et al., 2010). However, these models still cannot resolve small-scale GWs (<∼200 km horizontal wavelength), limited by their spatial resolutions and current computing power. There is a clear and pressing need for high-resolution, global observations of the transient and episodic GW spectrum reaching the mesosphere (Miller et al., 2015).

The NASA Atmospheric Waves Experiment (AWE) mission was launched to the International Space Station (ISS) in November 2023 with the goal of characterizing the properties of global mesospheric GWs. AWE operates an Advanced Mesospheric Temperature Mapper (AMTM), a ∼600 km-wide-field-of-view infrared imager, to measure several spectral lines in the airglow emission of the hydroxyl (3,1) and (2,0) bands (layer altitude ∼87 km) every second with 2 km horizontal resolution. The AMTM combines infrared detector technology and high throughput optical systems, making high-quality GW temperature mapping possible from space. Details about the AMTM can be found in Pautet et al. (2014). The ISS completes ∼15.5 orbits per day, with the orbit progressing by ∼5.625° per day and by ∼22.5 min in local time. The AMTM images GWs near the nighttime mesopause between ±55° latitude with partial longitudinal coverage each day, and full nocturnal longitudinal coverage every 4 days. At higher latitudes (±47–52°), AMTM imagery allows GWs to be imaged on 2 or 3 successive orbits, over 2 or 3 successive days, and nearly continuously in longitude. This enables high temporal sensitivity to major midlatitude GW hotspot sources including orography, frontal systems, and jet streams.

Two major sudden stratospheric warmings (SSWs) occurred during the winter of 2023 and 2024, after the AWE instrument was launched. SSWs are large-scale meteorological phenomenon in the polar winter stratosphere, characterized by rapid increases in temperature over several days (Butler et al., 2015). The disturbances in the stratosphere could significantly modify the propagation of GWs, leading to notable changes in the thermal and wind structure of the MLT (Vincent, 2015). One mechanism is when westward propagating GWs become saturated at lower altitudes due to Doppler shifting to shorter vertical wavelengths by reduced eastward wind or reversal to westward wind, GWs in the stratosphere are weakened (Lindzen, 1981). Another mechanism is the background wind filtering near the critical layer, which inhibits the vertical propagation of GWs with phase speeds less than the background wind. Weakened GW activity in the stratosphere after a SSW has been shown in ground-based observations (Thurairajah et al., 2010) and spaced-based observations (Harvey et al., 2023; Kogure et al., 2021; Wright et al., 2010; Xu et al., 2018), as well as in model simulations (e.g., Liu, 2017; Siskind et al., 2010; Yamashita et al., 2010).

However, studies of GWs in the mesosphere during and after SSW events have mostly focused on large-scale GWs using limb scan satellite data. Yamashita et al. (2013) showed an enhancement of GW activity at 80 km

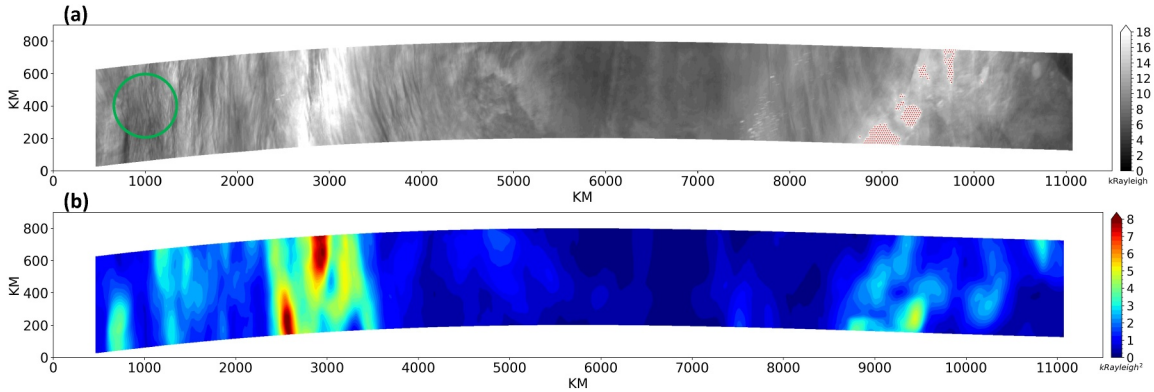

Figure 1. Radiance data for the first orbit of the AWE $Q_1(1)$ emission line on 22 November 2023. (a) Radiance, and (b) radiance variance, computed based on surrounding pixels within a 200 km radius, as indicated by the green circle. The red dots in panel (a) represent pixels potentially impacted by high-altitude clouds, identified by values within 20°S–20°N that exceed two standard deviations of the entire swath.

before the formation of the elevated stratopause immediately following 2006 and 2009 SSW events, as observed by the SABER. Thurairajah et al. (2014) using Solar Occultation for Ice Experiment (SOFIE) data from 2009 to 2013 reported highly variable GW activity at 80 km during different SSWs. Ern et al. (2016) investigated a number of SSW events from 2002 to 2014 and found strong suppression in GW activity when the zonal wind is reversed from eastward to westward, based on SABER and HIRDLS data. Nayak and Yiğit (2019) demonstrated a decrease in GW amplitudes during the 2009 SSW in the altitude range of 65–100 km as retrieved from SABER observations. However, SABER measures waves with horizontal wavelengths longer than ∼200 km. GWs with short horizontal wavelengths are not captured. The AWE mission provides an opportunity to directly observe small-scale (30–300 km) GW activity in the mesosphere on a global scale, allowing us to investigate how SSWs modulate mesospheric GWs. The remainder of the paper is organized as follows. Section 2 provides the data description. Section 3 presents temporal and spatial GW variations observed by AWE during the 2024 SSW events. Furthermore, the role of background winds in affecting GWs is discussed. Conclusions are presented in Section 4.

2. Data

2.1. The Atmospheric Waves Experiment (AWE) Data

AWE measures emissions from the near-infrared OH band, the most prominent nighttime airglow emission from Earth's mesopause region. OH nocturnal emission typically originates in a well-defined layer centered at ∼87 km, with a full width, half maximum of ∼7 km (Baker & Stair, 1988). OH airglow is sensitive to waves with vertical wavelengths greater than the layer thickness (i.e., >8 km) and horizontal wavelengths ranging from several kilometers to thousands of kilometers along track. AWE is capable of capturing GWs (scales range from 30 to 300 km) that are the most influential drivers of the MLT. The AMTM deployed for the AWE mission has four identical telescopes that simultaneously measure the $P_1(2)$, and $P_1(4)$ emission lines of the (3,1) band, the $Q_1(1)$ line of the (2,0) band, along with the nearby atmospheric background. Signals from these four cameras are used to derive temperature at ∼87 km.

In this study, orbital keograms of radiance data from the $Q_1(1)$ emission line are used to examine how SSWs impact mesospheric GW activity. Radiance data from the $Q_1(1)$ emission line are preferred as the focus of this investigation is primarily on qualitative results. In the future, temperature, once the calibration is finalized, will be used to provide a more quantitative perspective. The swath data are ∼600 km wide and ∼15,000 km long for each orbit with a 2 km horizontal resolution. The radiance for the first orbit on 22 November 2023 is shown in Figure 1a. The $Q_1(1)$ emission line is less sensitive to the OH reflection off the ground and clouds because of the strong water vapor absorption at the same wavelength. However, some high-altitude clouds due to deep convection are still visible in the data. To avoid their potential impacts on GWs, pixels within 20°S–20°N (deep convection region) with values exceeding two standard deviations of the entire swath are discarded, indicated as red dots in panel a. In addition, pixels contaminated by sources on the ground (e.g., city lights, oil rigs) are also discarded. Subsequently, GW variance (Figure 1b) for each pixel is computed based on surrounding pixels within

a 200-km radius (indicated as the green circle in panel a), capturing waves with wavelengths shorter than 400 km. Every day, the data from each orbit are binned into 1° × 1° grid to form a daily map.

2.2. The Modern-Era Retrospective Analysis for Research and Applications, Version 2 (MERRA-2) Data

To understand the dynamical mechanism between GW variations and the background wind field, meteorological data from NASA's Modern-Era Retrospective Analysis for Research and Applications Version 2 (MERRA-2) data products were utilized. MERRA-2 is a NASA meteorological reanalysis data product that enables the use of modern hyperspectral radiance and microwave observations and includes updates to the Goddard Earth Observing System (GEOS) model and analysis scheme (Gelaro et al., 2017). MERRA-2 assimilates the MLS-retrieved temperature profiles at altitudes above 5 hPa to constrain the dynamics of the stratopause and lower mesosphere (Gelaro et al., 2017). However, the temperature errors in MLS observations start to increase above the lower mesosphere. The data are provided twice daily with a horizontal resolution of 0.5° latitude by 0.625° longitude on 42 pressure levels that extend from the Earth's surface to ∼65 km altitude (Global Modeling and Assimilation Office, 2015). The data products include various meteorological parameters (e.g., wind and temperature) along with several other atmospheric diagnostics. In the context of this study, temperature and zonal wind data have been averaged daily to characterize the SSW.

3. Results and Discussion

3.1. Characteristics of the 2023/2024 SSWs

Two major Arctic SSW events are identified during the 2023/2024 winter, following the criteria established by Charlton and Polvani (2007). The onset of a major SSW event is defined as the day when zonally averaged zonal wind reverses from eastward to westward at 60°N and 10 hPa between 1 November and 31 March. The onsets of the two major SSWs are 16 January 2024, and 4 March 2024, based on MERRA-2 zonal wind data. The dates are consistent with those identified using the European Center for Medium-Range Weather Forecasts (Lee et al., 2024). Both events are categorized as displacement SSWs according to the criteria from B. G. Song et al. (2020), where the amplitude of the zonal wavenumber 1 geopotential height perturbation at 65°N and 10 hPa is larger than the respective zonal wavenumber 2 amplitude from 7 days prior and after the onset.

Figure 2 shows the time-altitude cross-sections of zonally averaged daily mean zonal wind at 60°N (panel a) and temperature averaged over 70°N–90°N (panel b) using MERRA-2. Positive (negative) values represent eastward (westward) zonal wind. During the 2023 and 2024 winter, the stratosphere and mesosphere in the polar region were frequently disturbed. Two major SSWs took place on 16 January 2024 and 4 March 2024, indicated by vertical gray lines. The wind reversal was accompanied by polar warming in the stratosphere. However, these two events exhibited different evolution patterns. The wind reversal at 10 hPa was brief, lasting only 1 day during the January SSW event. In contrast, it lasted for 21 days during the March event and propagated to lower altitudes during the subsequent warming period. The zonal wind above 1 hPa returned eastward after 5 and 11 days during the January and March SSW events, respectively. Note that the eastward zonal-mean zonal wind between 35 and 60 km over the polar region weakened and transitioned to westward on 2 January and 14 February. These events were accompanied by polar warming and classified as minor SSW events since the wind reversals did not reach 10 hPa.

3.2. Effects of SSWs on GW Activity

The dominant sources of GWs in the middle atmosphere differ between winter and summer hemisphere (M. J. Alexander & Grimsdell, 2013; Sato et al., 2009). Convective GWs dominate the summer hemisphere, where Rossby waves or orographic GWs cannot propagate up to the mesopause region due to westward background winds. In contrast, in the winter hemisphere, the dominant GW sources are steep mountains and strong westerly jets.

Figure 3 shows the daily evolution of AWE GW activity (panel a) and its anomaly with respect to the 2-month average (panel b), as a function of latitude. The gaps in the Northern Hemisphere (NH) during mid-December and early February are due to periods of high beta angle of the ISS. Yellow (magenta) contours are 50 km zonal-mean MERRA-2 wind speed values of 30 m/s (50 m/s). NH midlatitude GW activity at ∼87 km was strong from 20 December 2023 to 2 January 2024, 7 January 2024 to 15 January 2024, 23 January 2024 to 31 January 2024, and 23 March 2024 to 31 March 2024. During these periods, zonal wind in the stratosphere was strongly eastward.

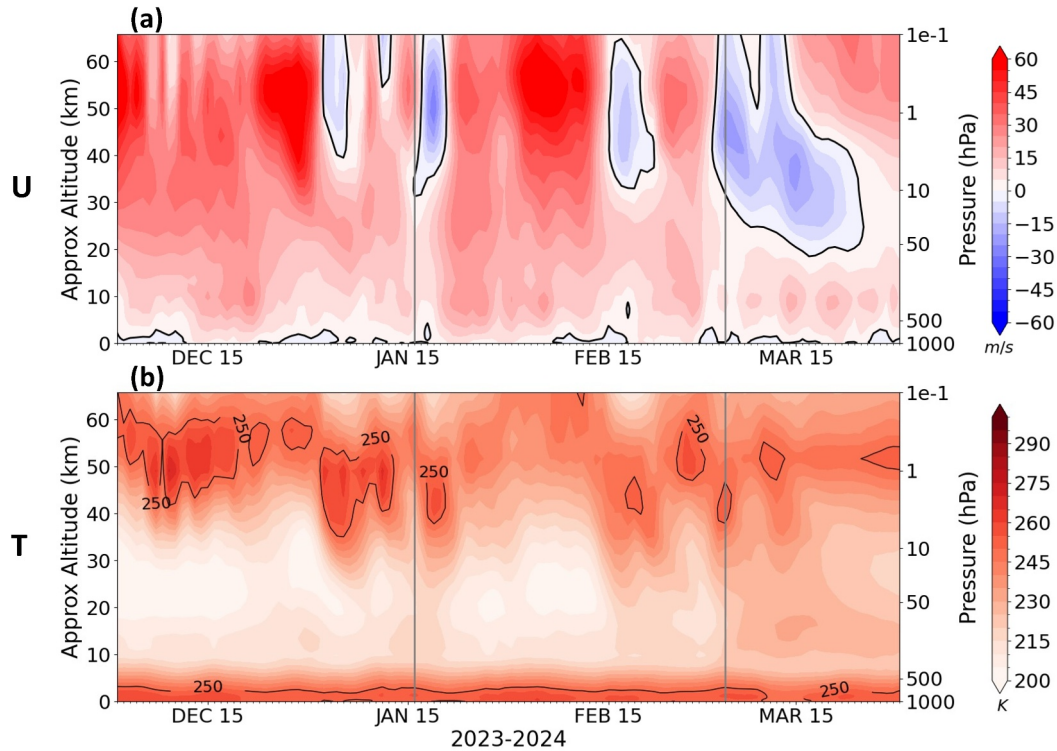

Figure 2. Time-altitude section of zonal-mean (a) zonal wind (m/s) and temperature (K) from MERRA-2. The onsets of SSW are 16 January 2024 and 4 March 2024 (vertical gray lines). Zonal wind is at 60°N and temperature is averaged from 70°N to 90°N. The *x*-axis is date from 1 December 2023.

This is consistent with a variety of GW observations in the stratosphere (e.g., Hindley et al., 2020; Yoshiki et al., 2004), and mesosphere (e.g., Ern et al., 2018; Harvey et al., 2023; Jiang et al., 2006; Wu & Waters, 1996b).

The intense oscillation of stratospheric winds during SSWs could impact the propagation of GWs. Reduced GW activity was observed at ~87 km after the onsets of two major SSWs in 2024 (Figure 3). The decreased GW activity lasted longer during the March SSW event due to the extended duration of zonal wind reversal. Depressed GW activity also occurred on 2 January and 25 February, associated with the weakening of the zonal wind.

The distribution of GWs strongly depends on the zonal and meridional shape of the background wind field (Ern et al., 2016). Figure 4 shows the longitude-latitude dependence of radiance variance averaged over 5 days. Yellow and magenta contours mark the 0 and 25 m/s zonal wind at 50 km, respectively. During 11–15 January, strong GW activity at 87 km was observed over the Pacific Ocean, the United States, and the Eurasian continent, where the zonal wind was strongly eastward (panel a). Once SSWs occurred (18–22 January), the stratospheric zonal wind at high latitudes in the NH weakened or reversed at specific longitudes. As a result, GWs generally became weaker globally (panel b). On the other hand, GWs appeared over North Africa following the onset of the SSW, which were excited by the polar vortex.

In late winter, mesospheric GW activity was observed over the United States and the Pacific Ocean where the zonal wind was eastward (panel c). NH GW activity was generally weaker in March compared to January, which could be associated with changes in the zonal wind field in late winter (line contours in Figures 3 and 4). The eastward wind weakened and shifted to westward over the Eurasian continent, leading to weaker GW activity during 28 February to 3 March compared to 11–15 January (panels a and c). Following the onset of the March SSW, the eastward wind over western longitudes in the NH weakened, leading to reduced GW activity (panel d).

3.3. Possible Mechanisms

Background wind plays an important role in the vertical propagation of GWs. Figure 5a shows 45°N MERRA-2 zonal-mean zonal wind at 50 km (solid black line) and AWE GW activity at ~87 km (dashed red line).

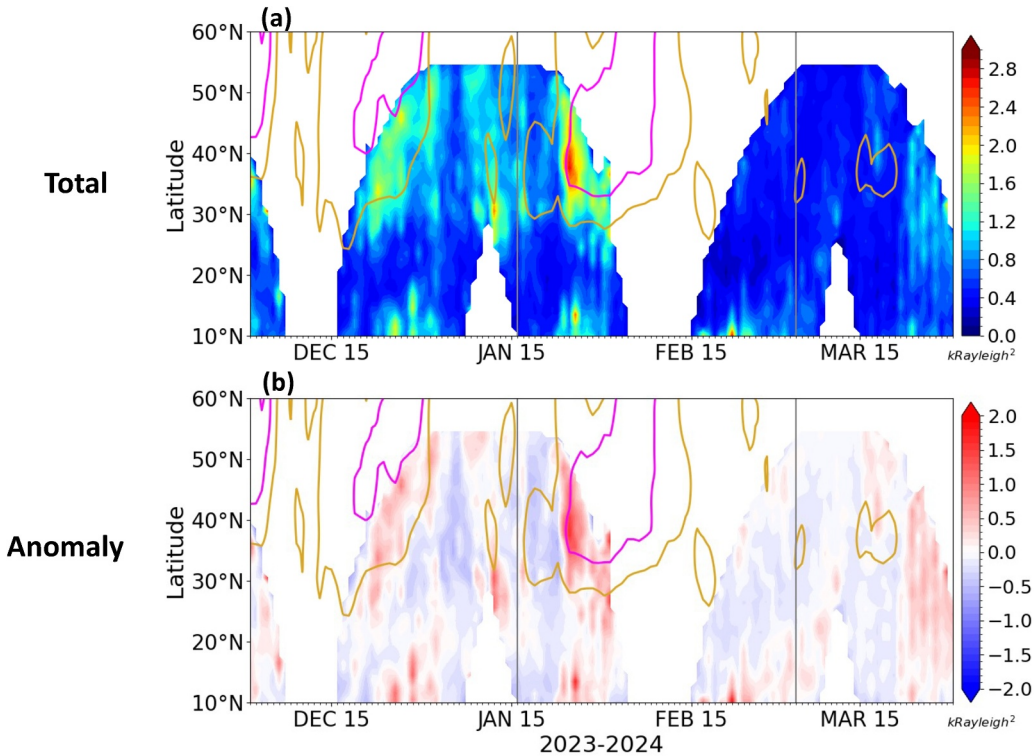

Figure 3. Time-latitude cross section of the (a) radiance variance, and (b) radiance variance anomaly at ~87 km during the 2024 SSW events. Line contours indicate zonal-mean MERRA-2 wind speed values of 30 m/s (yellow) and 50 m/s (magenta) at 50 km.

Mesospheric GW activity was positively correlated with zonal wind in the lower mesosphere during the 2023 and 2024 winter, which might be associated with the flow adjustment as noted in Yamashita et al. (2010) and Liu (2017). In particular, AWE GW activity was dramatically reduced as the zonal wind weakened. GW variance rebounded more quickly and to a larger extent following the January SSW event. This is consistent with the faster recovery of the zonal wind in the upper stratosphere compared to the prolonged weak zonal wind in the middle and lower stratosphere following the March SSW event (Figure 2a).

The vertical profiles of MERRA-2 zonal wind at 45°N, 90°E during the January and March SSW event are shown in Figures 5b and 5c, respectively. December–March mean is represented by solid black lines, while daily values

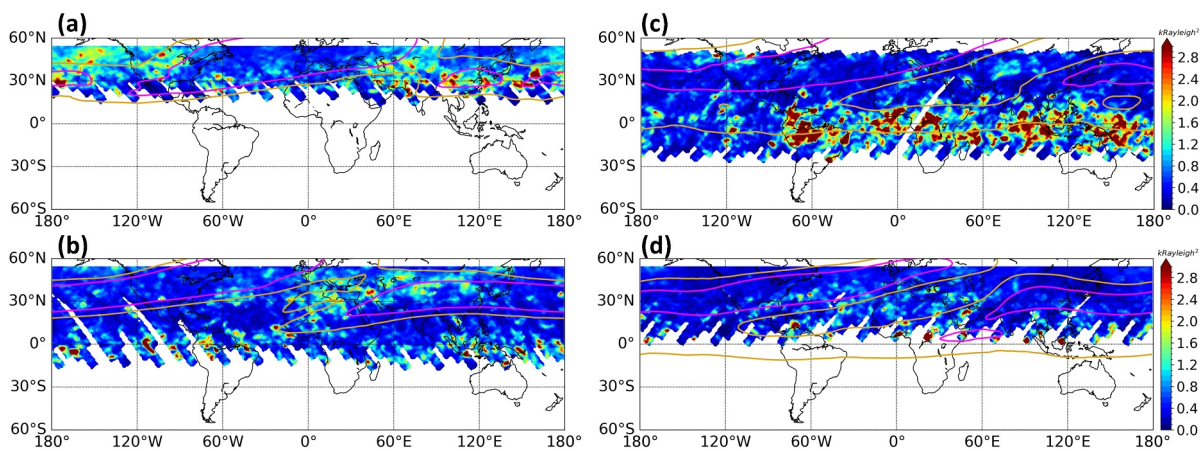

Figure 4. Map of the radiance variance on (a) 11–15 January, (b) 18–22 January, (c) 28 February to 3 March, and (d) 6–10 March at 87 km. Yellow and magenta line contours indicate 0 and 25 m/s MERRA-2 zonal wind at 50 km.

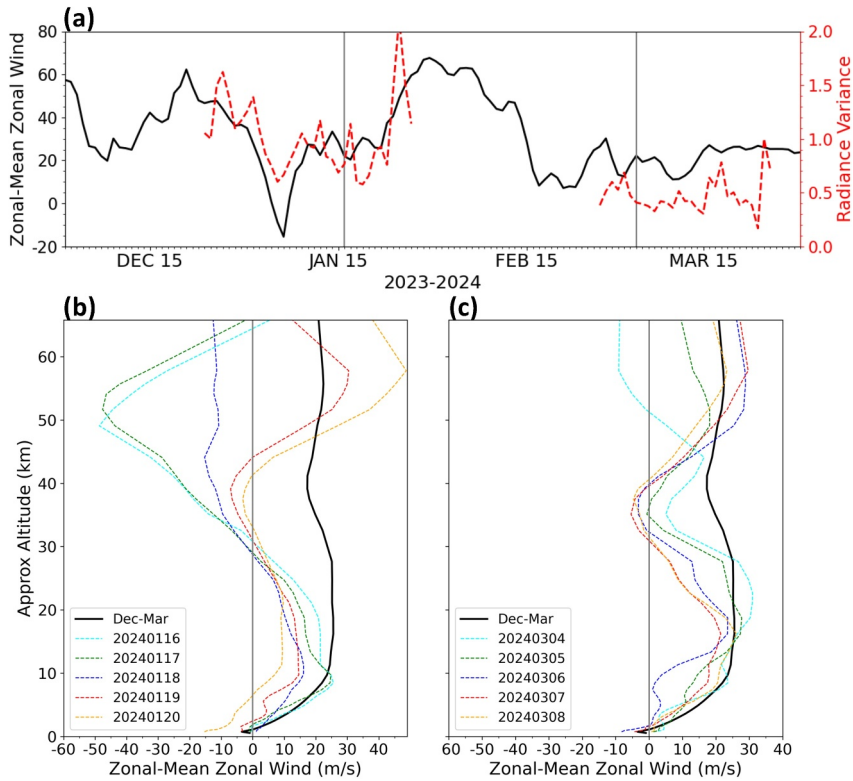

Figure 5. Time series of the MERRA-2 zonal-mean zonal wind in m/s at 50 km (black solid lines) and AWE radiance variance in kRayleigh^2 (red dashed lines) at 45°N (a). The profile of zonal wind at 45°N, 90°E in wintertime (b and c).

following the onset are shown with dashed colored lines. Wintertime zonal wind was eastward from the surface up to the lower mesosphere, peaking at approximately 25 km with an amplitude of 30 m/s. The background wind allows GWs with westward phases to propagate upward, reaching the mesopause region, and probably break there (Holton, 1982). Following the onset of the January SSW event (16 January to 18 January), the eastward zonal wind in the altitude range of 30–60 km reversed to westward, filtering out the upward propagating GWs. As the zonal wind recovered to eastward after 19 January (panel b), GW activity increased (panel a). The March SSW event exhibited a similar feature (panel c). However, the zonal wind reversal at 45°N was weaker and occurred at lower altitude (~35 km). We note that the stronger GW variation during the January SSW event compared to the March event may be associated with the greater background wind variation in the former.

4. Conclusions

The NASA AWE instrument measures several spectral lines in the airglow emission of the hydroxyl (3,1) and (2,0) bands at layer altitude ~87 km, providing direct observation of small-scale GWs in the upper mesosphere on a global scale. AWE can capture GWs in the spectrum of 30–300 km generated from various tropospheric sources such as orography, jet stream, and convection. The AWE data collection started on 22 November 2023. This work examined the variation of GW activity during the two major 2024 SSW events using AWE data. In addition, MERRA-2 was used to understand the dynamical mechanism linking GW variations to the background wind field. The main findings of our research are as follows.

- The variations of GW activity in the mesosphere showed an evident correlation with the magnitude of stratospheric zonal wind. AWE observed high GW activity in regions where the stratospheric zonal wind was strong.
- Northern Hemisphere (NH) mid-high latitude GW activity during the two major SSW events shared similarities. Following the onset of SSWs, NH midlatitude GW activity at ~87 km was reduced.

- The decline in GW activity was most likely caused by wind filtering and wave saturation. The upward propagation of GWs was suppressed when the zonal wind reversed from eastward to westward in the upper stratosphere. Based on the theory, in regions where the eastward zonal wind weakens, GWs tend to refract to shorter vertical wavelengths, leading to saturation at lower altitudes. Future work will focus on diagnosing the sources and propagation conditions of GWs.

The AWE mission sheds light on the spatial and temporal variation of GWs at around 87 km. The data will be useful for validating GW characteristics simulated in high-resolution global circulation models. Combination of high-resolution global circulation models and AWE observations is promising for precise understanding of global GW activity.

Data Availability Statement

NASA AWE data are accessible at https://awe.physics.usu.edu/data/download/. $Q_1(1)$ intensity swaths correspond to Level-3c. MERRA-2 data are from Global Modeling and Assimilation Office (2015).

Acknowledgments
J.Z., Y.Z, D.P, L.S, M.T and H.L. acknowledge support by the NASA under Contract Number 80GSFC18C0007. National Center for Atmospheric Research is a major facility sponsored by the National Science Foundation under Cooperative Agreement No. 1852977.

References

Alexander, M. J., Gille, J., Cavanaugh, C., Coffey, M., Craig, C., Eden, T., et al. (2008). Global estimates of gravity wave momentum flux from High Resolution Dynamics Limb Sounder observations. *Journal of Geophysical Research*, *113*(D15). https://doi.org/10.1029/2007jd008807

Alexander, M. J., & Grimsdell, A. W. (2013). Seasonal cycle of orographic gravity wave occurrence above small islands in the Southern Hemisphere: Implications for effects on the general circulation. *Journal of Geophysical Research: Atmospheres*, *118*(20), 11–589. https://doi.org/10.1002/2013jd020526

Alexander, S. P., Klekociuk, A. R., & Murphy, D. J. (2011). Rayleigh lidar observations of gravity wave activity in the winter upper stratosphere and lower mesosphere above Davis, Antarctica (69°S, 78°E). *Journal of Geophysical Research*, *116*(D13), D13109. https://doi.org/10.1029/2010jd015164

Andrews, D. G., Holton, J. R., & Leovy, C. B. (1987). *Middle atmosphere dynamics (No. 40)*. Academic Press.

Azeem, I., Yue, J., Hoffmann, L., Miller, S. D., Straka, W. C., III., & Crowley, G. (2015). Multisensor profiling of a concentric gravity wave event propagating from the troposphere to the ionosphere. *Geophysical Research Letters*, *42*(19), 7874–7880. https://doi.org/10.1002/2015gl065903

Baker, D. J., & Stair, A. T., Jr. (1988). Rocket measurements of the altitude distributions of the hydroxyl airglow. *Physica Scripta*, *37*(4), 611–622. https://doi.org/10.1088/0031-8949/37/4/021

Beatty, T. J., Hostetler, C. A., & Gardner, C. S. (1992). Lidar observations of gravity waves and their spectra near the mesopause and stratopause at Arecibo. *Journal of the Atmospheric Sciences*, *49*(6), 477–496. https://doi.org/10.1175/1520-0469(1992)049<0477:loogwa>2.0.co;2

Becker, E., & Vadas, S. E. (2018). Secondary gravity waves in the winter mesosphere: Results from a high-resolution global circulation model. *Journal of Geophysical Research: Atmospheres*, *123*(5), 2605–2627. https://doi.org/10.1002/2017JD027460

Beldon, C. L., & Mitchell, N. J. (2009). Gravity waves in the mesopause region observed by meteor radar, 2: Climatologies of gravity waves in the Antarctic and Arctic. *Journal of Atmospheric and Solar-Terrestrial Physics*, *71*(8–9), 875–884. https://doi.org/10.1016/j.jastp.2009.03.009

Beldon, C. L., & Mitchell, N. J. (2010). Gravity wave–tidal interactions in the mesosphere and lower thermosphere over Rothera, Antarctica (68°S, 68°W). *Journal of Geophysical Research*, *115*(D18). https://doi.org/10.1029/2009jd013617

Butler, A. H., Seidel, D. J., Hardiman, S. C., Butchart, N., Birner, T., & Match, A. (2015). Defining sudden stratospheric warmings. *Bulletin of the American Meteorological Society*, *96*(11), 1913–1928. https://doi.org/10.1175/bams-d-13-00173.1

Cao, B., & Liu, A. Z. (2022). Statistical characteristics of high-frequency gravity waves observed by an airglow imager at Andes Lidar Observatory. *Earth and Space Science*, *9*(6), e2022EA002256. https://doi.org/10.1029/2022ea002256

Chanin, M. L., & Hauchecorne, A. (1981). Lidar observation of gravity and tidal waves in the stratosphere and mesosphere. *Journal of Geophysical Research*, *86*(C10), 9715–9721. https://doi.org/10.1029/jc086ic10p09715

Charlton, A. J., & Polvani, L. M. (2007). A new look at stratospheric sudden warmings. Part I: Climatology and modeling benchmarks. *Journal of Climate*, *20*(3), 449–469. https://doi.org/10.1175/jcli3996.1

De la Torre, A., Tsuda, T., Hajj, G. A., & Wickert, J. (2004). A global distribution of the stratospheric gravity wave activity from GPS occultation profiles with SAC-C and CHAMP. *Journal of the Meteorological Society of Japan Series II*, *82*(1B), 407–417. https://doi.org/10.2151/jmsj.2004.407

Dowdy, A. J., Vincent, R. A., Tsutsumi, M., Igarashi, K., Murayama, Y., Singer, W., & Murphy, D. J. (2007). Polar mesosphere and lower thermosphere dynamics: 1. Mean wind and gravity wave climatologies. *Journal of Geophysical Research*, *112*(D17). https://doi.org/10.1029/2006jd008126

Ern, M., Hoffmann, L., & Preusse, P. (2017). Directional gravity wave momentum fluxes in the stratosphere derived from high-resolution AIRS temperature data. *Geophysical Research Letters*, *44*(1), 475–485. https://doi.org/10.1002/2016gl072007

Ern, M., Preusse, P., Alexander, M. J., & Warner, C. D. (2004). Absolute values of gravity wave momentum flux derived from satellite data. *Journal of Geophysical Research*, *109*(D20). https://doi.org/10.1029/2004jd004752

Ern, M., Preusse, P., Gille, J. C., Hepplewhite, C. L., Mlynczak, M. G., Russell, J. M., III., & Riese, M. (2011). Implications for atmospheric dynamics derived from global observations of gravity wave momentum flux in stratosphere and mesosphere. *Journal of Geophysical Research*, *116*(D19), D19107. https://doi.org/10.1029/2011jd015821

Ern, M., Trinh, Q. T., Kaufmann, M., Krisch, I., Preusse, P., Ungermann, J., et al. (2016). Satellite observations of middle atmosphere gravity wave absolute momentum flux and of its vertical gradient during recent stratospheric warmings. *Atmospheric Chemistry and Physics*, *16*(15), 9983–10019. https://doi.org/10.5194/acp-16-9983-2016

Ern, M., Trinh, Q. T., Preusse, P., Gille, J. C., Mlynczak, M. G., Russell, J. M., III., & Riese, M. (2018). GRACILE: A comprehensive climatology of atmospheric gravity wave parameters based on satellite Limb soundings. *Earth System Science Data*, *10*(2), 857–892. https://doi.org/10.5194/essd-10-857-2018

Fetzer, E. J., & Gille, J. C. (1994). Gravity wave variance in LIMS temperatures. Part I: Variability and comparison with background winds. *Journal of the Atmospheric Sciences*, *51*(17), 2461–2483. https://doi.org/10.1175/1520-0469(1994)051<2461:gwvilt>2.0.co;2

Fritts, D. C., & Alexander, M. J. (2003). Gravity wave dynamics and effects in the middle atmosphere. *Reviews of Geophysics*, *41*(1). https://doi.org/10.1029/2001rg000106

Gelaro, R., McCarty, W., Suárez, M. J., Todling, R., Molod, A., Takacs, L., et al. (2017). The modern-era retrospective analysis for research and applications, version 2 (MERRA-2). *Journal of Climate*, *30*(14), 5419–5454. https://doi.org/10.1175/jcli-d-16-0758.1

Global Modeling and Assimilation Office (GMAO). (2015). MERRA-2 inst6_3d_ana_Np: 3d,6-Hourly,Instantaneous,Pressure-Level,Analysis, Analyzed Meteorological Fields V5.12.4, Greenbelt, MD, USA [Dataset]. *Goddard Earth Sciences Data and Information Services Center (GES DISC)*. https://doi.org/10.5067/A7S6XP56VZWS

Harvey, V. L., Randall, C. E., Goncharenko, L. P., Becker, E., Forbes, J. M., Carstens, J., et al. (2023). CIPS observations of gravity wave activity at the edge of the polar vortices and coupling to the ionosphere. *Journal of Geophysical Research: Atmospheres*, *128*(12), e2023JD038827. https://doi.org/10.1029/2023jd038827

Hecht, J. H., Liu, A. Z., Fritts, D. C., Walterscheid, R. L., Gelinas, L. J., & Rudy, R. J. (2023). A "boreing" night of observations of the upper mesosphere and lower thermosphere over the Andes Lidar Observatory. *Journal of Geophysical Research: Atmospheres*, *128*(20), e2023JD038754. https://doi.org/10.1029/2023jd038754

Hibbins, R. E., Espy, P. J., Jarvis, M. J., Riggin, D. M., & Fritts, D. C. (2007). A climatology of tides and gravity wave variance in the MLT above Rothera, Antarctica obtained by MF radar. *Journal of Atmospheric and Solar-Terrestrial Physics*, *69*(4–5), 578–588. https://doi.org/10.1016/j.jastp.2006.10.009

Hindley, N. P., Wright, C. J., Hoffmann, L., Moffat-Griffin, T., & Mitchell, N. J. (2020). An 18-year climatology of directional stratospheric gravity wave momentum flux from 3-D satellite observations. *Geophysical Research Letters*, *47*(22), e2020GL089557. https://doi.org/10.1029/2020GL089557

Hoffmann, L., Spang, R., Orr, A., Alexander, M. J., Holt, L. A., & Stein, O. (2016). A decadal satellite record of gravity wave activity in the lower stratosphere to study polar stratospheric cloud formation. *Atmospheric Chemistry and Physics Discussions*, *2016*, 1–33.

Hoffmann, L., Xue, X., & Alexander, M. J. (2013). A global view of stratospheric gravity wave hotspots located with Atmospheric Infrared Sounder observations. *Journal of Geophysical Research: Atmospheres*, *118*(2), 416–434. https://doi.org/10.1029/2012jd018658

Holton, J. R. (1982). The role of gravity wave induced drag and diffusion in the momentum budget of the mesosphere. *Journal of the Atmospheric Sciences*, *39*(4), 791–799. https://doi.org/10.1175/1520-0469(1982)039<0791:trogwi>2.0.co;2

Holton, J. R. (1983). The influence of gravity wave breaking on the general circulation of the middle atmosphere. *Journal of the Atmospheric Sciences*, *40*(10), 2497–2507. https://doi.org/10.1175/1520-0469(1983)040<2497:tiogwb>2.0.co;2

Hozumi, Y., Saito, A., Sakanoi, T., Yue, J., Yamazaki, A., & Liu, H. (2024). Geographical and seasonal variations of gravity wave activities in the upper mesosphere measured by space-borne imaging of molecular oxygen nightglow. *Earth Planets and Space*, *76*(1), 66. https://doi.org/10.1186/s40623-024-01993-x

Jiang, J. H., Eckermann, S. D., Wu, D. L., & Wang, D. Y. (2006). Inter-annual variation of gravity waves in the Arctic and Antarctic winter middle atmosphere. *Advances in Space Research*, *38*(11), 2418–2423. https://doi.org/10.1016/j.asr.2005.09.036

Kim, Y. J., Eckermann, S. D., & Chun, H. Y. (2003). An overview of the past, present and future of gravity-wave drag parametrization for numerical climate and weather prediction models. *Atmosphere-Ocean*, *41*(1), 65–98. https://doi.org/10.3137/ao.410105

Kogure, M., Yue, J., & Liu, H. (2021). Gravity wave weakening during the 2019 Antarctic stratospheric sudden warming. *Geophysical Research Letters*, *48*(8), e2021GL092537. https://doi.org/10.1029/2021gl092537

Lee, S. H., Butler, A. H., & Manney, G. L. (2024). *Two major sudden stratospheric warmings during winter 2023/2024*. Weather.

Li, T., Leblanc, T., McDermid, I. S., Wu, D. L., Dou, X., & Wang, S. (2010). Seasonal and interannual variability of gravity wave activity revealed by long-term lidar observations over Mauna Loa Observatory, Hawaii. *Journal of Geophysical Research*, *115*(D13). https://doi.org/10.1029/2009jd013586

Li, Z., Robinson, W., & Liu, A. Z. (2009). Sources of gravity waves in the lower stratosphere above South Pole. *Journal of Geophysical Research*, *114*(D14). https://doi.org/10.1029/2008jd011478

Lindzen, R. S. (1981). Turbulence and stress owing to gravity wave and tidal breakdown. *Journal of Geophysical Research*, *86*(C10), 9707–9714. https://doi.org/10.1029/jc086ic10p09707

Liu, H. L. (2017). Gravity wave variation from the troposphere to the lower thermosphere during a stratospheric sudden warming event: A case study. *SOLA*, *13*, 24–30. https://doi.org/10.2151/sola.13a-005

Liu, H.-L., Lauritzen, P. H., Vitt, F., & Goldhaber, S. (2024). Assessment of gravity waves from tropopause to thermosphere and ionosphere in high-resolution WACCM-X simulations. *Journal of Advances in Modeling Earth Systems*, *16*(6), e2023MS004024. https://doi.org/10.1029/2023MS004024

Liu, H.-L., McInerney, J. M., Santos, S., Lauritzen, P. H., Taylor, M. A., & Pedatella, N. M. (2014). Gravity waves simulated by high-resolution whole atmosphere community climate model. *Geophysical Research Letters*, *41*(2014GL062468), 9106–9112. https://doi.org/10.1002/2014GL062468

McLandress, C., Alexander, M. J., & Wu, D. L. (2000). Microwave Limb Sounder observations of gravity waves in the stratosphere: A climatology and interpretation. *Journal of Geophysical Research*, *105*(D9), 11947–11967. https://doi.org/10.1029/2000jd900097

Miller, S. D., Straka, W. C., III., Yue, J., Smith, S. M., Alexander, M. J., Hoffmann, L., et al. (2015). Upper atmospheric gravity wave details revealed in nightglow satellite imagery. *Proceedings of the National Academy of Sciences of the United States of America*, *112*(49), E6728–E6735. https://doi.org/10.1073/pnas.1508084112

Mitchell, N. J., & Beldon, C. L. (2009). Gravity waves in the mesopause region observed by meteor radar: 1. A simple measurement technique. *Journal of Atmospheric and Solar-Terrestrial Physics*, *71*(8–9), 866–874. https://doi.org/10.1016/j.jastp.2009.03.011

Nayak, C., & Yiğit, E. (2019). Variation of small-scale gravity wave activity in the ionosphere during the major sudden stratospheric warming event of 2009. *Journal of Geophysical Research: Space Physics*, *124*(1), 470–488. https://doi.org/10.1029/2018ja026048

Pautet, P. D., Taylor, M. J., Pendleton, W. R., Zhao, Y., Yuan, T., Esplin, R., & McLain, D. (2014). Advanced mesospheric temperature mapper for high-latitude airglow studies. *Applied Optics*, *53*(26), 5934–5943. https://doi.org/10.1364/ao.53.005934

Perwitasari, S., Sakanoi, T., Yamazaki, A., Otsuka, Y., Hozumi, Y., Akiya, Y., et al. (2015). Coordinated airglow observations between IMAP/VISI and a ground-based all-sky imager on concentric gravity wave in the mesopause. *Journal of Geophysical Research: Space Physics*, *120*(11), 9706–9721. https://doi.org/10.1002/2015ja021424

Preusse, P., Dörnbrack, A., Eckermann, S. D., Riese, M., Schaeler, B., Bacmeister, J. T., et al. (2002). Space-based measurements of stratospheric mountain waves by CRISTA 1. Sensitivity, analysis method, and a case study. *Journal of Geophysical Research*, *107*(D23), CRI–6. https://doi.org/10.1029/2001jd000699

Preusse, P., Eckermann, S. D., Ern, M., Oberheide, J., Picard, R. H., Roble, R. G., et al. (2009). Global ray tracing simulations of the SABER gravity wave climatology. *Journal of Geophysical Research*, *114*(D8). https://doi.org/10.1029/2008jd011214

Preusse, P., Eckermann, S. D., & Offermann, D. (2000). Comparison of global distributions of zonal-mean gravity wave variance inferred from different satellite instruments. *Geophysical Research Letters*, *27*(23), 3877–3880. https://doi.org/10.1029/2000gl011916

Preusse, P., Schaeler, B., Bacmeister, J. T., & Offermann, D. (1999). Evidence for gravity waves in CRISTA temperatures. *Advances in Space Research*, *24*(11), 1601–1604. https://doi.org/10.1016/s0273-1177(99)00885-6

Randall, C. E., Carstens, J., France, J. A., Harvey, V. L., Hoffmann, L., Bailey, S. M., et al. (2017). New AIM/CIPS global observations of gravity waves near 50–55 km. *Geophysical Research Letters*, *44*(13), 7044–7052. https://doi.org/10.1002/2017gl073943

Sato, K. (2000). Sources of gravity waves in the polar middle atmosphere. *Advances in Polar Upper Atmosphere Research*, *14*, 233–240.

Sato, K., Watanabe, S., Kawatani, Y., Tomikawa, Y., Miyazaki, K., & Takahashi, M. (2009). On the origins of mesospheric gravity waves. *Geophysical Research Letters*, *36*(19). https://doi.org/10.1029/2009gl039908

Sato, K., & Yoshiki, M. (2008). Gravity wave generation around the polar vortex in the stratosphere revealed by 3-hourly radiosonde observations at Syowa Station. *Journal of the Atmospheric Sciences*, *65*(12), 3719–3735. https://doi.org/10.1175/2008jas2539.1

Siskind, D. E., Eckermann, S. D., McCormack, J. P., Coy, L., Hoppel, K. W., & Baker, N. L. (2010). Case studies of the mesospheric response to recent minor, major, and extended stratospheric warmings. *Journal of Geophysical Research*, *115*(D3). https://doi.org/10.1029/2010jd014114

Song, B. G., Chun, H. Y., & Song, I. S. (2020). Role of gravity waves in a vortex-split sudden stratospheric warming in January 2009. *Journal of the Atmospheric Sciences*, *77*(10), 3321–3342. https://doi.org/10.1175/jas-d-20-0039.1

Song, B. G., Song, I. S., Chun, H. Y., Lee, C., Kam, H., Kim, Y. H., et al. (2021). Activities of small-scale gravity waves in the upper mesosphere observed from meteor radar at King Sejong Station, Antarctica (62.22°S, 58.78°W) and their potential sources. *Journal of Geophysical Research: Atmospheres*, *126*(10), e2021JD034528. https://doi.org/10.1029/2021jd034528

Song, I. S., Lee, C., Kim, J. H., Jee, G., Kim, Y. H., Choi, H. J., et al. (2017). Meteor radar observations of vertically propagating low-frequency inertia-gravity waves near the southern polar mesopause region. *Journal of Geophysical Research: Space Physics*, *122*(4), 4777–4800. https://doi.org/10.1002/2016ja022978

Taylor, M. J., Pautet, P. D., Fritts, D. C., Kaifler, B., Smith, S. M., Zhao, Y., et al. (2019). Large-amplitude mountain waves in the mesosphere observed on 21 June 2014 during DEEPWAVE: 1. Wave development, scales, momentum fluxes, and environmental sensitivity. *Journal of Geophysical Research: Atmospheres*, *124*(19), 10364–10384. https://doi.org/10.1029/2019jd030932

Thurairajah, B., Bailey, S. M., Cullens, C. Y., Hervig, M. E., & Russell, J. M., III. (2014). Gravity wave activity during recent stratospheric sudden warming events from SOFIE temperature measurements. *Journal of Geophysical Research: Atmospheres*, *119*(13), 8091–8103. https://doi.org/10.1002/2014jd021763

Thurairajah, B., Collins, R. L., Harvey, V. L., Lieberman, R. S., Gerding, M., Mizutani, K., & Livingston, J. M. (2010). Gravity wave activity in the Arctic stratosphere and mesosphere during the 2007–2008 and 2008–2009 stratospheric sudden warming events. *Journal of Geophysical Research*, *115*(D3). https://doi.org/10.1029/2010jd014125

Tsuda, T., Nishida, M., Rocken, C., & Ware, R. H. (2000). A global morphology of gravity wave activity in the stratosphere revealed by the GPS occultation data (GPS/MET). *Journal of Geophysical Research*, *105*(D6), 7257–7273. https://doi.org/10.1029/1999jd901005

Vincent, R. A. (1994). Gravity-wave motions in the mesosphere and lower thermosphere observed at Mawson, Antarctica. *Journal of Atmospheric and Terrestrial Physics*, *56*(5), 593–602. https://doi.org/10.1016/0021-9169(94)90100-7

Vincent, R. A. (2015). The dynamics of the mesosphere and lower thermosphere: A brief review. *Progress in Earth and Planetary Science*, *2*, 1–13. https://doi.org/10.1186/s40645-015-0035-8

Vincent, R. A., & Fritts, D. C. (1987). A climatology of gravity wave motions in the mesopause region at Adelaide, Australia. *Journal of the Atmospheric Sciences*, *44*(4), 748–760. https://doi.org/10.1175/1520-0469(1987)044<0748:acogwm>2.0.co;2

Vincent, R. A., & Reid, I. M. (1983). HF Doppler measurements of mesospheric gravity wave momentum fluxes. *Journal of the Atmospheric Sciences*, *40*(5), 1321–1333. https://doi.org/10.1175/1520-0469(1983)040<1321:hdmomg>2.0.co;2

Wang, L., & Geller, M. A. (2003). Morphology of gravity-wave energy as observed from 4 years (1998–2001) of high vertical resolution US radiosonde data. *Journal of Geophysical Research*, *108*(D16). https://doi.org/10.1029/2002jd002786

Wang, L., Geller, M. A., & Alexander, M. J. (2005). Spatial and temporal variations of gravity wave parameters. Part I: Intrinsic frequency, wavelength, and vertical propagation direction. *Journal of the Atmospheric Sciences*, *62*(1), 125–142. https://doi.org/10.1175/jas-3364.1

Wilson, R., Chanin, M. L., & Hauchecorne, A. (1991). Gravity waves in the middle atmosphere observed by Rayleigh lidar: 2. Climatology. *Journal of Geophysical Research*, *96*(D3), 5169–5183. https://doi.org/10.1029/90jd02610

Wright, C. J., Osprey, S. M., Barnett, J. J., Gray, L. J., & Gille, J. C. (2010). High resolution dynamics Limb Sounder measurements of gravity wave activity in the 2006 Arctic stratosphere. *Journal of Geophysical Research*, *115*(D2). https://doi.org/10.1029/2009jd011858

Wu, D. L., & Waters, J. W. (1996a). Gravity-wave-scale temperature fluctuations seen by the UARS MLS. *Geophysical Research Letters*, *23*(23), 3289–3292. https://doi.org/10.1029/96gl02924

Wu, D. L., & Waters, J. W. (1996b). Satellite observations of atmospheric variances: A possible indication of gravity waves. *Geophysical Research Letters*, *23*(24), 3631–3634. https://doi.org/10.1029/96gl02907

Wu, D. L., & Waters, J. W. (1997). Observations of gravity waves with the UARS microwave Limb Sounder. In *Gravity wave processes: Their parameterization in global climate models* (pp. 103–120). Springer Berlin Heidelberg.

Xu, X., Yu, D., & Luo, J. (2018). The spatial and temporal variability of global stratospheric gravity waves and their activity during sudden stratospheric warming revealed by COSMIC measurements. *Advances in Atmospheric Sciences*, *35*(12), 1533–1546. https://doi.org/10.1007/s00376-018-5053-1

Yamashita, C., Chu, X., Liu, H. L., Espy, P. J., Nott, G. J., & Huang, W. (2009). Stratospheric gravity wave characteristics and seasonal variations observed by lidar at the South Pole and Rothera, Antarctica. *Journal of Geophysical Research*, *114*(D12). https://doi.org/10.1029/2008jd011472

Yamashita, C., England, S. L., Immel, T. J., & Chang, L. C. (2013). Gravity wave variations during elevated stratopause events using SABER observations. *Journal of Geophysical Research: Atmospheres*, *118*(11), 5287–5303. https://doi.org/10.1002/jgrd.50474

Yamashita, C., Liu, H. L., & Chu, X. (2010). Gravity wave variations during the 2009 stratospheric sudden warming as revealed by ECMWF-T799 and observations. *Geophysical Research Letters*, *37*(22). https://doi.org/10.1029/2010gl045437

Yoshiki, M., Kizu, N., & Sato, K. (2004). Energy enhancements of gravity waves in the Antarctic lower stratosphere associated with variations in the polar vortex and tropospheric disturbances. *Journal of Geophysical Research*, *109*(D23). https://doi.org/10.1029/2004jd004870

Yoshiki, M., & Sato, K. (2000). A statistical study of gravity waves in the polar regions based on operational radiosonde data. *Journal of Geophysical Research*, *105*(D14), 17995–18011. https://doi.org/10.1029/2000jd900204

Yuan, T., Heale, C. J., Snively, J. B., Cai, X., Pautet, P. D., Fish, C., et al. (2016). Evidence of dispersion and refraction of a spectrally broad gravity wave packet in the mesopause region observed by the Na lidar and Mesospheric Temperature Mapper above Logan, Utah. *Journal of Geophysical Research: Atmospheres*, *121*(2), 579–594. https://doi.org/10.1002/2015jd023685

Yue, J., Hoffmann, L., & Joan Alexander, M. (2013). Simultaneous observations of convective gravity waves from a ground-based airglow imager and the AIRS satellite experiment. *Journal of Geophysical Research: Atmospheres*, *118*(8), 3178–3191. https://doi.org/10.1002/jgrd.50341

Zhang, Y., Xiong, J., Liu, L., & Wan, W. (2012). A global morphology of gravity wave activity in the stratosphere revealed by the 8-year SABER/TIMED data. *Journal of Geophysical Research*, *117*(D21). https://doi.org/10.1029/2012jd017676